1-1-2010

Separation of the effects of astigmatic figure error from misalignments using Nodal Aberration Theory (NAT)

Tobias Schmid
University of Central Florida

Jannick P. Rolland
University of Central Florida

Andrew Rakich

Kevin P. Thompson

Separation of the effects of astigmatic figure error from misalignments using Nodal Aberration Theory (NAT)

Tobias Schmid,[1,*] Jannick P. Rolland,[2,1] Andrew Rakich,[3] and Kevin P. Thompson[4]

[1]*CREOL – The College of Optics and Photonics, University of Central Florida, Orlando, FL 32816, USA*
[2] *The Institute of Optics, University of Rochester, 275 Hutchison Rd., Rochester, NY 14627, USA*
[3] *Large Binocular Telescope Observatory, 933 N. Cherry Avenue, Tucson, AZ 85721, USA*
[4] *Optical Research Associates, 3 Graywood Lane, Pittsford, NY 14534, USA*
**tschmid@creol.ucf.edu*

Abstract: We present the nodal aberration field response of Ritchey-Chrétien telescopes to a combination of optical component misalignments and astigmatic figure error on the primary mirror. It is shown that both astigmatic figure error and secondary mirror misalignments lead to binodal astigmatism, but that each type has unique, characteristic locations for the astigmatic nodes. Specifically, the characteristic node locations in the presence of astigmatic figure error (at the pupil) in an otherwise aligned telescope exhibit symmetry with respect to the field center, i.e. the midpoint between the astigmatic nodes remains at the field center. For the case of secondary mirror misalignments, one of the astigmatic nodes remains nearly at the field center (in a coma compensated state) as presented in Optics Express 18, 5282-5288 (2010), while the second astigmatic node moves away from the field center. This distinction leads directly to alignment methods that preserve the dynamic range of the active wavefront compensation component.

OCIS codes: (080.0080) Geometric optics; (080.1010) Aberrations (global) (110.6770) Telescopes, (220.1140) Alignment, (220.1080) Active or Adaptive Optics.

References and links

1. K. P. Thompson, "Description of the third-order optical aberrations of near-circular pupil optical systems without symmetry," J. Opt. Soc. Am. A **22**(7), 1389–1401 (2005).
2. J. R. Rogers, "Techniques and tools for obtaining symmetrical performance from tilted-component systems," Opt. Eng. **39**(7), 1776–1787 (2000).
3. K. P. Thompson, T. Schmid, and J. P. Rolland, "The misalignment induced aberrations of TMA telescopes," Opt. Express **16**(25), 20345–20353 (2008).
4. T. Schmid, K. P. Thompson, and J. P. Rolland, "Misalignment-induced nodal aberration fields in two-mirror astronomical telescopes," Appl. Opt. **49**(16), D131–D144 (2010).
5. H. H. Hopkins, in *The Wave Theory of Aberrations* (Oxford on Clarendon Press, 1950).
6. R. A. Buchroeder, "Tilted component optical systems," Ph.D. dissertation (University of Arizona, 1976).
7. R. V. Shack, and K. Thompson, "Influence of alignment errors of a telescope system on its aberration field," Proc. SPIE **251**, 146–153 (1980).
8. T. Schmid, K. P. Thompson, and J. P. Rolland, "A unique astigmatic nodal property in misaligned Ritchey-Chrétien telescopes with misalignment coma removed," Opt. Express **18**(5), 5282–5288 (2010).
9. B. McLeod, "Collimation of Fast Wide-Field Telescopes," Publ. Astron. Soc. Pac. **108**, 217–219 (1996).
10. D. L. Terrett and W. J. Sutherland, "The interaction between pointing and active optics on the VISTA Telescope," presented at SPIE Astronomical Instrumentation, San Diego, CA, USA, 27 June - 2 July 2010.
11. R. N. Wilson, in *Reflecting Telescope Optics II* (Springer-Verlag, Berlin, 1999), Chap. 2.
12. K. P. Thompson, "Aberration Fields in Unobscured Mirror Systems," J. Opt. Soc. Am. **70**, 1603 (1980).
13. K. P. Thompson, "The aberration fields of optical systems without symmetry", PhD dissertation, The University of Arizona, College of Optical Sciences, (1980).
14. C. R. Burch, "On the optical see-saw diagram," Mon. Not. R. Astron. Soc. **103**, 159–165 (1942).
15. J. C. Wyant, and K. Creath, "Basic Wavefront Aberration Theory for Optical Metrology," in *Applied Optics and Optical Engineering, Vol. XI*, Academic Press (1992), Chap. 1.

#128812 - $15.00 USD Received 21 May 2010; revised 3 Jul 2010; accepted 13 Jul 2010; published 30 Jul 2010

16. K. P. Thompson, "Description of the third-order optical aberrations of near-circular pupil optical systems without symmetry: errata," J. Opt. Soc. Am. A **26**(3), 699–699 (2009).
17. K. P. Thompson, T. Schmid, O. Cakmakci, and J. P. Rolland, "Real-ray-based method for locating individual surface aberration field centers in imaging optical systems without rotational symmetry," J. Opt. Soc. Am. A **26**(6), 1503–1517 (2009).

1. Introduction

Nodal aberration theory for optical imaging systems without symmetry (but with rotationally symmetric components) has emerged as an effective approach to describe the aberrations in misaligned or intentionally decentered/tilted optical systems [1–3]. We have recently demonstrated that the theory is well suited for the development of deterministic alignment strategies for astronomical telescopes [4]. The work is based on the wave aberration theory of Hopkins [5], the concept of shifted aberration field centers attributed to Buchroeder [6], and a key insight from Shack [7] that combined lead to the discovery that many of the traditional aberration fields become multinodal when symmetry is broken.

Recently, we demonstrated that the application of nodal aberration theory to the common class of astronomical telescopes, Ritchey-Chrétien telescopes, leads to the discovery of a general property of misalignment induced binodal astigmatism in those telescopes, when misalignments have been partially compensated based on the removal of field-constant coma [8]. Specifically, it has been found that one of the two misalignment induced astigmatic nodes (points in the field with zero astigmatism) is effectively constrained to remain at the field center by the operation of removing misalignment induced field-constant coma. For the context of this discussion the field center or on-axis refers to the field point where the 0° input field central ray intersects the image plane. To reduce the complexity of the coordinate systems, it has been assumed that the position of the 0° field point on the detector has been established independently and this treatment will be presented elsewhere.

The remaining node is free to move to any point in the field, governed by a linear relationship between the orientation of the optical axis of the secondary mirror with respect to the optical axis of the primary mirror (the optical axis is the line connecting the center of curvature with the center of rotational symmetric departure of the aspheric/conic from the spherical mirror surface).

An emerging challenge in astronomy is to integrate active optics into the imaging chain of the telescope creating an opportunity to correct for residual figure error in the primary mirror, which will often be a segmented component in the future. McLeod [9] has suggested previously that astigmatism caused by poor primary mirror support will add an additional contribution to the nominal + misalignment-induced astigmatism. He indicated that primary mirror support induced contributions to astigmatism can be obtained by including additional parameters in the non-linear least square fitting algorithm utilized when computing the secondary mirror rotation angles about the coma-free pivot point [9]. As pointed out by a reviewer, very recent work (unpublished at the time of submission of this manuscript) on extracting the mount induced contribution to astigmatism can be found in Terrett and Sutherland [10].

In this paper we describe how to integrate an astigmatic primary mirror figure error characterized by a Zernike polynomial description for the case of a monolithic mirror into nodal aberration theory, providing an intuitive understanding of the effects of primary mirror support induced astigmatism on the astigmatic aberration field. With this integration we show a new characteristic nodal behavior; the introduction of primary mirror figure error results in each astigmatic node moving equally away from the center of the field of view. Incorporating the primary mirror figure error term into the analytic equations that predict the location of the astigmatic nodes facilitates the ability to systematically isolate performance degradation caused by astigmatic mirror figure error from that caused by the state of secondary mirror alignment, which is the key result of this paper. The ability to decouple astigmatism caused by figure error and misalignments is critical for the emerging class of 21st century astronomical

#128812 - $15.00 USD Received 21 May 2010; revised 3 Jul 2010; accepted 13 Jul 2010; published 30 Jul 2010

and military telescopes with active full aperture figure compensation. By distinguishing misalignment from figure error induced effects, some of the consequences of compensating misalignments with an active wavefront correcting component, and vice versa, can be avoided. For example, compensating one with the other typically leads to a lateral decenter of the exit-pupil and an inclination of the exit beam to the primary mirror optical axis [11], requiring not only focus but also tilt adjustments of the focal plane. As discussed by Wilson, some of the consequences can be dealt with by utilizing pointing software, but it is more effective to prevent the cause for these additional steps, to the extent possible, in the first place. By isolating these two causes of telescope performance degradation, the misalignments of the secondary mirror and the residual astigmatic figure error in the primary mirror, the dynamic range of the active optics system can be reserved for figure correction only, consequently extending the performance envelope for the telescope.

2. Formulating Nodal Aberration Theory of a misaligned Ritchey-Chrétien telescope with astigmatic figure error on the primary mirror

In this work, astigmatic figure error on the primary mirror (coincident with the stop) of a Ritchey-Chrétien telescope will be introduced in nodal aberration theory, which, until now, has been limited to modeling optical systems with rotationally symmetric surfaces (or portions thereof). This set of conditions is more restrictive than necessary, but, by imposing them here, they can provide a succinct development of this fundamental concept. The introduction of primary mirror figure error will be accomplished by adding the corresponding low order astigmatic Zernike polynomial characterization of the surface error to the wave aberration expression, extended to the vector form for optical systems that are not rotationally symmetric as developed in [1].

The key observation leading to how to integrate mirror figure error with the nodal aberration theory of misaligned optical systems is to consider the equations of nodal aberration theory for the special case of an aspheric surface placed at an aperture stop [12]. As developed in Appendix C of [13], consider a 3rd order (4th order in wavefront) aspheric plate corrector, as in a Schmidt telescope, placed in the entrance/exit-pupil. When this aspheric plate is decentered by an amount $\Delta\boldsymbol{\rho}$, a normalized vector, which is the ratio of the displacement to the aperture diameter, the resulting new additive vector wave aberration terms are those beyond the first term in Eq. (1), given by

$$\begin{aligned} W &= W_{040}[(\boldsymbol{\rho}+\Delta\boldsymbol{\rho})\bullet(\boldsymbol{\rho}+\Delta\boldsymbol{\rho})]^2 \\ &= W_{040}[(\boldsymbol{\rho}\bullet\boldsymbol{\rho})^2 + 4(\Delta\boldsymbol{\rho}\bullet\boldsymbol{\rho})(\boldsymbol{\rho}\bullet\boldsymbol{\rho}) + 4(\Delta\boldsymbol{\rho}\bullet\Delta\boldsymbol{\rho})(\boldsymbol{\rho}\bullet\boldsymbol{\rho}) \\ &\quad + 2(\Delta\boldsymbol{\rho}^2\bullet\boldsymbol{\rho}^2) + 4(\Delta\boldsymbol{\rho}\bullet\Delta\boldsymbol{\rho})(\Delta\boldsymbol{\rho}\bullet\boldsymbol{\rho}) + (\Delta\boldsymbol{\rho}\bullet\Delta\boldsymbol{\rho})^2], \end{aligned} \tag{1}$$

where W_{040} denotes the wave aberration for spherical aberration, $\boldsymbol{\rho}$ is a normalized vector that denotes a location in the exit-pupil and $\Delta\boldsymbol{\rho}$ is the normalized offset of the rotationally symmetric conic/aspheric plate from the optical axis. When the aspheric contribution to the wavefront is placed in a pupil and then decentered relative to the stop/pupil, the original contribution (exclusively) to spherical aberration generates lower order aberration components, including astigmatism, that are each themselves constant over the field of view, since the beam footprints of all field points on the surface are identical [14]. In fact, for large decenters of a rotationally symmetric parent aspheric relative to the portion illuminated by the beam, the dominant aberration is astigmatism, which is the aberration to be developed exclusively here because it is typically the dominant residual figure error in a large monolithic primary mirror due to variation in mount stresses with mirror orientation with respect to gravity, which occurs in-use at an observatory. Referring to the form for astigmatism in a misaligned optical system presented in Eq. (4).2) and Eq. (4).13) of [1] (see also Eq. (12) below), it can be seen that the contribution to astigmatism in Eq. (1) comes from the fourth

#128812 - $15.00 USD Received 21 May 2010; revised 3 Jul 2010; accepted 13 Jul 2010; published 30 Jul 2010

term; $2(\Delta\boldsymbol{\rho}^2 \bullet \boldsymbol{\rho}^2)$. In Eq. (1), term one continues as the surface contribution to spherical aberration, which is unchanged, the second term is a new surface contribution to coma, which is constant with field, $\Delta\boldsymbol{\rho}$ replacing $\boldsymbol{H}$, and the third term is a new field constant surface contribution to field curvature (it is differentiated from term four by the fact that it is a scalar and not a vector term). The fourth term is the new field constant contribution to astigmatism, which is the term that has been identified as a path that can be used to integrate directly the influence of astigmatic figure errors on the primary mirror with nodal aberration theory. Continuing with Eq. (1), term five is a field constant contribution to distortion and term six represents a field constant piston term.

Figure 1 shows an example of how a rotationally symmetric spherical aberration contribution evolves to a comatic dominated contribution for a small decenter as shown in Fig. 1(c) and then as a dominantly astigmatic wavefront term as shown in Fig. 1d for a larger decenter relative to the center of the aperture stop (or its image). Reference [12] and Appendix C of [13] provide the mathematical details that introduce and describe the developments that provide the framework describing each of the field constant aberrations that are introduced by an offset aperture. Within that framework, here we are choosing to look only at an astigmatic form of figure error because at least until recently it has been the most common, and as a result we are using only the 4th term in Eq. (1) as the mechanism for the introduction of a field constant astigmatic mirror figure error. This approach to introducing figure error then enables the addition of optical surfaces that in general are not rotationally symmetric. Here we limit this development to small astigmatic deviations to the ideal conic/aspheric surface of the primary mirror of a Ritchey-Chrétien telescope.

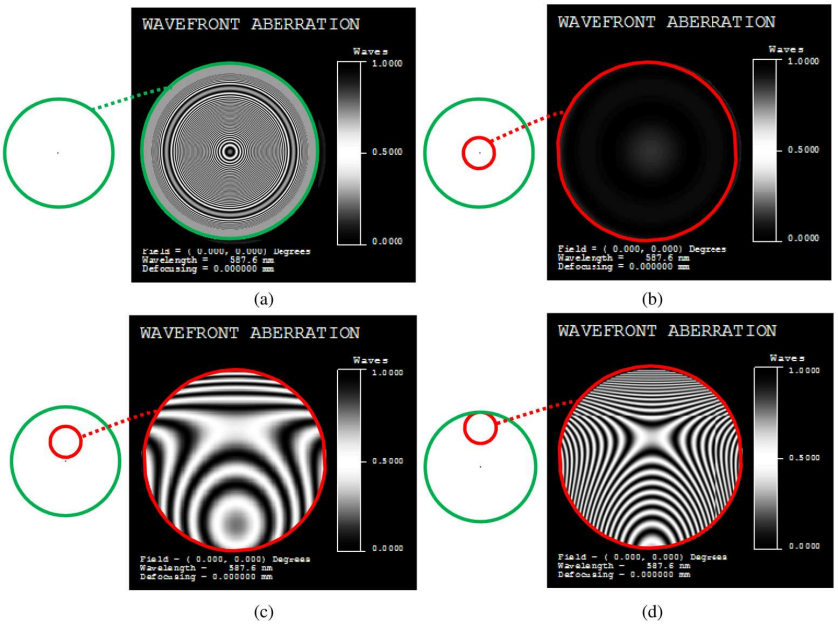

Fig. 1. Aspheric corrector plate with aperture stop positions (a) centered on the optical axis utilizing the full aperture indicating spherical aberration, (b) centered on the optical axis utilizing only a small portion of the aperture, (c,d) shifted aperture stop, causing field-constant astigmatism.

Having identified an access point within the context of nodal aberration theory of misaligned optical systems where the concept and mathematics of a misfigured mirror (or more generally any nonrotationally symmetric optical surface placed at the stop or in a pupil)

#128812 - $15.00 USD Received 21 May 2010; revised 3 Jul 2010; accepted 13 Jul 2010; published 30 Jul 2010

can be inserted, consider first a common representation of a misfigured mirror, an interferogram, as the quantitative data source. An interferogram of the primary mirror that contains and displays the departure from the aspheric/conic surface of the nominal design for the surface, as if it was tested on-axis in a null configuration, is an effective and practical method for quantifying the figure error of the primary mirror. This can be considered as an aspheric surface contribution that was presented as Eq. (1) in the context of this development. An example interferogram is shown in Fig. 2, which has an astigmatic error (and a focus term). This interferometric data, which is readily measured at, in particular, the on-axis field point, is typically quantified based on the value of the FRINGE Zernike coefficients, a form of Zernike polynomial commonly used in the interferometric testing industry.

The simulated interferogram of Fig. 2 can be parameterized based on the measured Zernike polynomial coefficient values for terms C_5 and C_6. With these measured/simulated values, the magnitude, ${}_{(FIGERR)}C_{5,6}$, and orientation, ${}_{(FIGERR)}\xi^{*}_{5,6}$, of the astigmatic error in the wavefront due to the residual state of the primary mirror figure is given by

$$ {}_{(FIGERR)}C_{5,6} = \sqrt{\left({}_{(FIGERR)}C_5\right)^2 + \left({}_{(FIGERR)}C_6\right)^2}, \tag{2} $$

$$ {}_{(FIGERR)}\xi^{*}_{5,6} = \frac{1}{2} ArcTan\left(\frac{\left({}_{(FIGERR)}C_6\right)}{\left({}_{(FIGERR)}C_5\right)}\right). \tag{3} $$

Referring to the FRINGE version of the Zernike polynomial, the polynomial dependence for the low order astigmatic terms from [15] are given by

$$ {}_{(FIGERR)}Z_5 = {}_{(FIGERR)}C_5\rho^2\cos(2\phi), \tag{4} $$

$$ {}_{(FIGERR)}Z_6 = {}_{(FIGERR)}C_6\rho^2\sin(2\phi), \tag{5} $$

where ρ is the radial variable describing the corresponding zone in the exit-pupil, and ϕ describes the azimuthal frequency, with sign conventions as shown in Fig. 3(a), i.e. the azimuthal dependence is measured from the positive ρ_x axis. The radial and azimuthal dependence as shown in Eq. (4)-(5) is notably exactly the dependence obtained as the result of the vector multiplication, which is the basis for nodal aberration theory [16],

$$ \boldsymbol{\rho}^2 = \rho^2\begin{pmatrix}\sin(2\phi)\\ \cos(2\phi)\end{pmatrix}, \tag{6} $$

with

$$ \boldsymbol{\rho} = \rho e^{j\phi}, \tag{7} $$

where a different orientation of the ρ_x axis and a different reference for the azimuthal dependence (from the ρ_y axis) are assumed as shown in Fig. 3(b). Since the interferograms in this work are shown in the same coordinate system as used for the aberration field vectors in nodal aberration theory, there is a sign reversal in Eq. (3), which is then given by

$$ {}_{(FIGERR)}\xi_{5,6} = \frac{1}{2} ArcTan\left(\frac{-\left({}_{(FIGERR)}C_6\right)}{\left({}_{(FIGERR)}C_5\right)}\right). \tag{8} $$

Although only the astigmatic term is presented here, any Zernike polynomial term that is placed on a surface in a pupil or at the stop can be accommodated with this methodology. For surfaces away from the pupil or the stop, even though not further discussed in this paper, the

#128812 - $15.00 USD Received 21 May 2010; revised 3 Jul 2010; accepted 13 Jul 2010; published 30 Jul 2010

approach can be extended to take the specific pupil footprint for each field at the particular surface into account, which introduces among other effects a field dependence of the figure error contributions, in general.

To integrate an astigmatic figure error at the pupil into the existing characterization of the misalignment induced aberration fields it is only necessary to label this contribution as a figure error component (*FIGERR*) and add it directly to the existing astigmatic component that is independent of the field of view and has a squared vector behavior, given by

$$\boldsymbol{B}_{222}^{2} = {}_{(MISALIGN)}\boldsymbol{B}_{222}^{2} + {}_{(FIGERR)}\boldsymbol{B}_{222}^{2}, \tag{9}$$

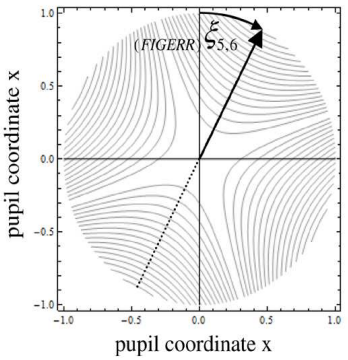

$${}_{(RC,ALIGNED,FIGERR)}W = \frac{1}{2}\left[W_{222}\boldsymbol{H}^{2} + {}_{(FIGERR)}\boldsymbol{B}_{222}^{2}\right] \bullet \boldsymbol{\rho}^{2}$$

$${}_{(FIGERR)}\boldsymbol{B}_{222}^{2} \equiv 2\left({}_{(FIGERR)}C_{5,6}\right)\exp\left[\, j2\left({}_{(FIGERR)}\xi_{5,6}\right)\right]$$

$${}_{(FIGERR)}C_{5,6} = \sqrt{\left({}_{(FIGERR)}C_{5}\right)^{2} + \left({}_{(FIGERR)}C_{6}\right)^{2}}$$

$${}_{(FIGERR)}\xi_{5,6} = \frac{1}{2}ArcTan\left(\frac{-\left({}_{(FIGERR)}C_{6}\right)}{\left({}_{(FIGERR)}C_{5}\right)}\right)$$

Fig. 2. Interferogram characterizing the primary mirror astigmatic figure error.

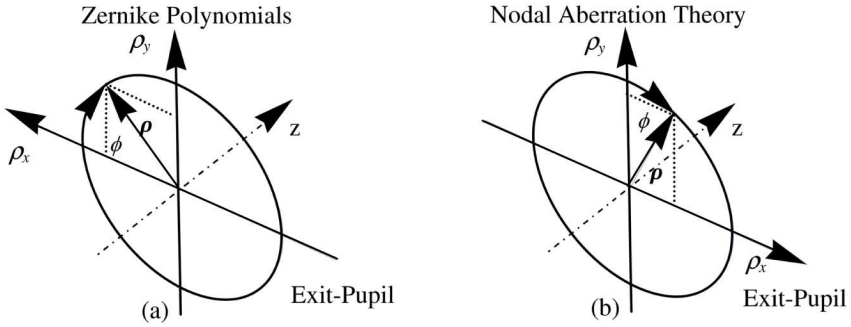

Fig. 3. Coordinate system definition in the exit-pupil, showing (a) the definition for the FRINGE Zernike polynomials, and (b) the coordinate system orientation utilized in nodal aberration theory.

where

$${}_{(FIGERR)}\boldsymbol{B}_{222}^{2} \equiv 2\left({}_{(FIGERR)}C_{5,6}\right)\exp\left[\, j2\left({}_{(FIGERR)}\xi_{5,6}\right)\right], \tag{10}$$

$${}_{(MISALIGN)}\boldsymbol{B}_{222}^{2} \equiv W_{222,SM}^{(SPH)}\boldsymbol{\sigma}_{SM}^{2(SPH)} + W_{222,SM}^{(ASPH)}\boldsymbol{\sigma}_{SM}^{2(ASPH)}, \tag{11}$$

where $\boldsymbol{\sigma}_{SM}^{(SPH)}$, $\boldsymbol{\sigma}_{SM}^{(ASPH)}$ are vectors that result from the tilt and/or decenter of the secondary mirror relative to the optical axis of the primary mirror and that point to the location of the rotationally symmetric aberration field contributions of the secondary mirror for the spherical base surface (*SPH*) and aspheric component (*ASPH*) in the image field, as discussed in [17].

Comparing Fig. 2 and Fig. 4(a) illustrates the interrelationship of the interferogram data and the construction of the nodal vector component ${}_{(FIGERR)}\boldsymbol{B}_{222}^{2}$. Specifically, the angle

#128812 - $15.00 USD Received 21 May 2010; revised 3 Jul 2010; accepted 13 Jul 2010; published 30 Jul 2010

describing the orientation of the vector ${}_{(FIGERR)}\boldsymbol{B}_{222}^2$ in Fig. 4(a) is twice the angle describing the orientation of the interferogram.

Utilizing Eq. (9)-(11) the total wave aberration of a misaligned Ritchey-Chrétien telescope with primary mirror astigmatic figure error, aligned to remove field-constant coma and ignoring the field curvature term is given by [1]

$$ {}_{(RC,MISALIGN,FIGERR)}W = W_{AST} = \frac{1}{2}W_{222}[(\boldsymbol{H}-\boldsymbol{a}_{222})^2 + \boldsymbol{b}_{222}^2]\bullet\boldsymbol{\rho}^2, \tag{12} $$

$$ \boldsymbol{b}_{222}^2 \equiv \frac{\boldsymbol{B}_{222}^2}{W_{222}} - \boldsymbol{a}_{222}^2, \tag{13} $$

$$ \boldsymbol{B}_{222}^2 = {}_{(MISALIGN)}\boldsymbol{B}_{222}^2 + {}_{(FIGERR)}\boldsymbol{B}_{222}^2. \tag{14} $$

$$ \boldsymbol{a}_{222} \equiv \frac{\boldsymbol{A}_{222}}{W_{222}}, \tag{15} $$

$$ \boldsymbol{A}_{222} \equiv W_{222,SM}^{(SPH)}\boldsymbol{\sigma}_{SM}^{(SPH)} + W_{222,SM}^{(ASPH)}\boldsymbol{\sigma}_{SM}^{(ASPH)}, \tag{16} $$

where $\boldsymbol{a}_{222}$ denotes the midpoint between the two astigmatic nodes, $\boldsymbol{b}_{222}$ is related to the distance between the astigmatic nodes, ${}_{(MISALIGN)}\boldsymbol{B}_{222}^2$ is given in Eq. (11), ${}_{(FIGERR)}\boldsymbol{B}_{222}^2$ is given in Eq. (10), and $W_{222,SM}^{(SPH)}$ and $W_{222,SM}^{(ASPH)}$ are the astigmatic wave aberration coefficients for the secondary mirror, separated into spherical base sphere and aspheric/conic contributions, respectively.

3. Binodal response of the astigmatic field dependence of a Ritchey-Chrétien telescope with primary mirror astigmatic figure error: ${}_{(MISALIGN)}\boldsymbol{B}_{222}^2 = \boldsymbol{0}$; ${}_{(FIGERR)}\boldsymbol{B}_{222}^2 \neq \boldsymbol{0}$

Before treating the more general case of the combination of misalignment with figure error, the astigmatic binodal response to astigmatic figure error applied to the primary mirror of a Ritchey-Chrétien telescope will be presented. In the case of an aligned Ritchey-Chrétien telescope, ${}_{(MISALIGN)}\boldsymbol{a}_{222} = {}_{(MISALIGN)}\boldsymbol{B}_{222}^2 = \boldsymbol{0}$, with astigmatic figure error, ${}_{(FIGERR)}\boldsymbol{B}_{222}^2 \neq \boldsymbol{0}$, Eq. (12) reduces to

$$ {}_{(RC,ALIGN,FIGERR)}W = \frac{1}{2}\left[W_{222}\boldsymbol{H}^2 + {}_{(FIGERR)}\boldsymbol{B}_{222}^2\right]\bullet\boldsymbol{\rho}^2. \tag{17} $$

The locations of the astigmatic nodes are found by finding the zeros of Eq. (17), i.e. the positions in the field $\boldsymbol{H}$ for which ${}_{(RC,ALIGN,FIGERR)}W = 0$. For the Ritchey-Chrétien solution, which ensures that $W_{222} \neq 0$, this condition leads to

$$ \boldsymbol{H}^2 = -\frac{{}_{(FIGERR)}\boldsymbol{B}_{222}^2}{W_{222}}, \tag{18} $$

with the binodal solution

$$ \boldsymbol{H} = \pm i\frac{{}_{(FIGERR)}\boldsymbol{B}_{222}}{\sqrt{W_{222}}}, \tag{19} $$

#128812 - $15.00 USD Received 21 May 2010; revised 3 Jul 2010; accepted 13 Jul 2010; published 30 Jul 2010

using the methods of vector multiplication described in Appendix A of [1] and where $_{(FIGERR)}\boldsymbol{B}_{222}$ is computed from the astigmatic figure error measurement of the coefficients $_{(FIGERR)}C_5$ and $_{(FIGERR)}C_6$, which are then used in Eq. (2)-(5).

Equation (19) denotes two vectors pointing in opposing directions to each of the astigmatic nodes, significantly, originating from the field center ($\boldsymbol{a}_{222} = \mathbf{0}$). Consequently, in the case of an astigmatic figure error in an otherwise aligned Ritchey-Chrétien telescope (which is not corrected for field-quadratic astigmatism as an intrinsic property of the optical design form, i.e. $W_{222} \neq 0$), the two astigmatic nodes always exhibit symmetry with respect to the field center, as visualized in Figs. 4(a), 4(b). Note that for the case of a telescope design where the uncorrected astigmatism of the optical design is greater than zero, $W_{222} > 0$ the nodes emerge at ± 90° to the direction of the $\boldsymbol{B}_{222}$ vector, which is determined from the interferogram data. If one would apply the same concepts to optical systems where $W_{222} < 0$, the astigmatic nodes would emerge along the $\boldsymbol{B}_{222}$ vector, since in that case the minus sign in the denominator of Eq. (19) would contribute an additional 90°. An important characteristic of astigmatic figure errors at the aperture stop is that it is fully characterized by $\boldsymbol{B}_{222}$ and does not contribute to the $\boldsymbol{a}_{222}$ vector.

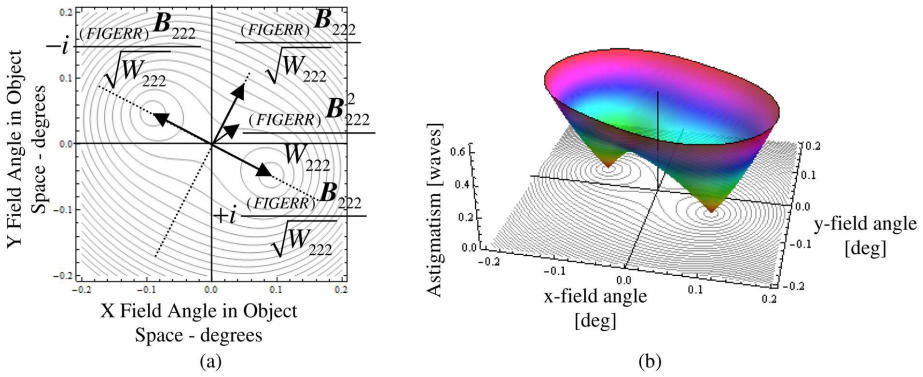

Fig. 4. (a) Binodal astigmatism caused by an astigmatic figure error on the primary mirror in the case of a fully aligned Ritchey-Chrétien telescope, and (b) the magnitude of astigmatism corresponding to (b).

4. Binodal response of the astigmatic field dependence of a Ritchey-Chrétien telescope with misalignments and astigmatic figure error: $_{(MISALIGN)}\boldsymbol{B}^2_{222} \neq \mathbf{0}$; $_{(FIGERR)}\boldsymbol{B}^2_{222} \neq \mathbf{0}$

While astigmatism in a Ritchey-Chrétien telescope becomes binodal in the presence of either misalignments or astigmatic figure errors, or both, in the case of astigmatic figure errors and misalignments, a characteristic difference in the nodal geometry allows separating the two effects, as will be presented in this section.

4.1. Conditions imposed as a result of aligning a Ritchey-Chrétien telescope to remove field-constant coma

It has been shown by the authors that the operation of removing field-constant coma does result in placing some important conditions on one of the node locations for binodal astigmatism [8]. Specifically, it has been shown that one of the astigmatic nodes remains essentially at the field center, caused by the secondary mirror coma contributions ($W^{(SPH)}_{131,SM}$ and

#128812 - $15.00 USD Received 21 May 2010; revised 3 Jul 2010; accepted 13 Jul 2010; published 30 Jul 2010

$W_{131,SM}^{(ASPH)}$), which are of equal sign and similar magnitude (Fig. 5(a)). Consequently, after the telescope has been aligned for zero constant coma, i.e.

$$W_{131,SM}^{(SPH)}\boldsymbol{\sigma}_{SM}^{(SPH)} + W_{131,SM}^{(ASPH)}\boldsymbol{\sigma}_{SM}^{(ASPH)} = \mathbf{0}, \tag{20}$$

the vectors $\boldsymbol{\sigma}_{SM}^{(SPH)}$ and $\boldsymbol{\sigma}_{SM}^{(ASPH)}$ are almost equal in length and point into opposite directions, as shown in Fig. 5(b). When calculating the quantity ${}_{(MISALIGN)}\boldsymbol{B}_{222}^{2} \equiv W_{222,SM}^{(SPH)}\boldsymbol{\sigma}_{SM}^{2(SPH)} + W_{222,SM}^{(ASPH)}\boldsymbol{\sigma}_{SM}^{2(ASPH)}$ it is found to be small for any realistic decenters and tilts, since the squared vectors $\boldsymbol{\sigma}_{SM}^{2(SPH)}$ and $\boldsymbol{\sigma}_{SM}^{2(ASPH)}$ point into the same direction, while $W_{222,SM}^{(SPH)}$ and $W_{222,SM}^{(ASPH)}$ are opposite in sign and similar in magnitude. As result from Eq. (13), ${}_{(MISALIGN)}\boldsymbol{b}_{222}^{2} \cong -\boldsymbol{a}_{222}^{2}$ and the astigmatic nodes are located at $\boldsymbol{H} = \boldsymbol{a}_{222} \pm i\boldsymbol{b}_{222} = \left(\mathbf{0}, 2\boldsymbol{a}_{222}\right)$ [8].

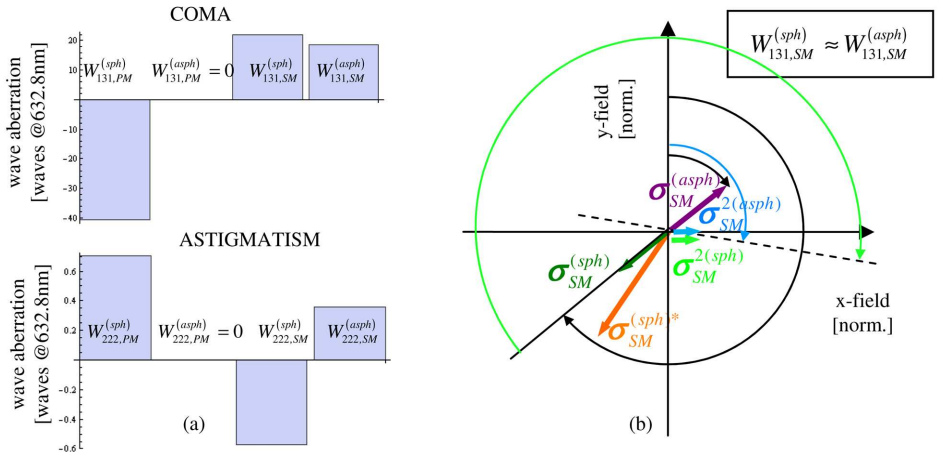

Fig. 5. (a) Wave aberration contributions for coma (top) and astigmatism (bottom), showing the spherical base curve and conic/aspheric surface contributions, (b) secondary mirror aberration field centers (spherical and aspheric) before (denoted by "*") and after removing misalignment induced coma. The example used here to demonstrate the theory is equivalent to the Ritchey-Chrétien configuration utilized in [8].

4.2. Conditions resulting from primary mirror astigmatic figure error and misalignments in a Ritchey-Chrétien telescope

Figure 6(b) illustrates a characteristic interferogram dominated by astigmatic figure error, which is the most common form of residual figure error on a monolithic primary mirror of a large astronomical telescope (see for example Fig. 6 of [1]). In parallel with Fig. 6(a), which is directly linked to the misalignment of the secondary mirror in a coma-corrected state, the residual figure error in the primary mirror is most commonly characterized by a Zernike polynomial decomposition of the measured wavefront on-axis during commissioning or in some cases during or just prior to operation, visualized in Fig. 6(b).

As stated in Eq. (12), the two vectors that control the node positions for misalignment/figure error induced binodal astigmatic field dependence are $\boldsymbol{a}_{222}$ and $\boldsymbol{b}_{222}^{2}$. The vector $\boldsymbol{a}_{222}$, shown in Fig. 7(a), determines the center of symmetry (planar) of the binodal astigmatic field. In this case, it is caused exclusively by secondary mirror misalignments and is computed from Eq. (15)-(16), using the wave aberration coefficients shown in Fig. 5(a) and the $\boldsymbol{\sigma}_{SM}^{(SPH,ASPH)}$ vectors shown in Fig. 5(b). As developed in Section 2 and 3, and a key to

#128812 - $15.00 USD Received 21 May 2010; revised 3 Jul 2010; accepted 13 Jul 2010; published 30 Jul 2010

distinguishing between secondary misalignment and astigmatic figure errors on the primary mirror, the astigmatic figure errors do not have a contribution to the $\boldsymbol{a}_{222}$-vector, illustrated in Fig. 7(b).

Figure 8 illustrates the other component contribution to the geometry of the nodes associated with binodal astigmatism, $\boldsymbol{b}^2_{222}$. This is the vector that decomposes to point from the center of biplanar symmetry located by $\boldsymbol{a}_{222}$ to the location of each node, which is symmetric about the end point of $\boldsymbol{a}_{222}$. Here, the alignment component of ${}_{(MISALIGN)}\boldsymbol{b}^2_{222}$ is shown in Fig. 8(a) for a misaligned Ritchey-Chrétien telescope that has been partially aligned for zero field-constant coma, as described in [8]. The ${}_{(FIGERR)}\boldsymbol{b}^2_{222} = {}_{(FIGERR)}\boldsymbol{B}^2_{222} / W_{222}$ contribution, which is a quantitative representation of the primary mirror figure error, is computed directly from the interferogram and the knowledge of W_{222} (from nominal system data) using Eq. (13)-(14), and is visualized in Fig. 8(b). The vectorial addition of secondary mirror misalignment contribution and the primary mirror astigmatic figure error contribution, ${}_{(MISALIGN)}\boldsymbol{b}^2_{222}$ and ${}_{(FIGERR)}\boldsymbol{b}^2_{222}$, respectively, is shown in Fig. 8(c) (as an illustration of Eq. (14)). By taking the square root of the final composite vector $\boldsymbol{b}^2_{222}$, the final vector $\boldsymbol{b}_{222}$ is obtained that determines the locations of the astigmatic nodes, as shown in Fig. 9(d).

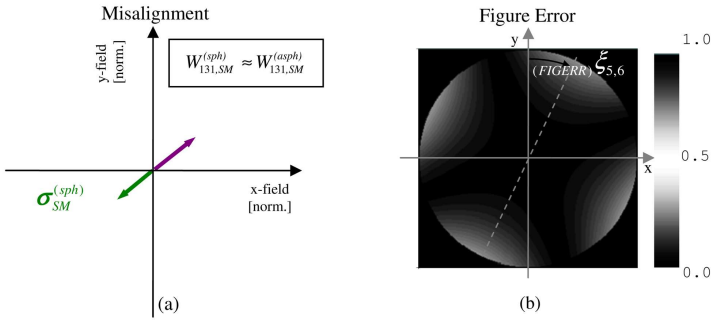

Fig. 6. (a) Aberration field centers for the spherical and aspheric aberration field contributions of the secondary mirror after aligning the telescope for zero field-constant coma. (b) Astigmatic primary mirror figure error for a Ritchey-Chrétien telescope.

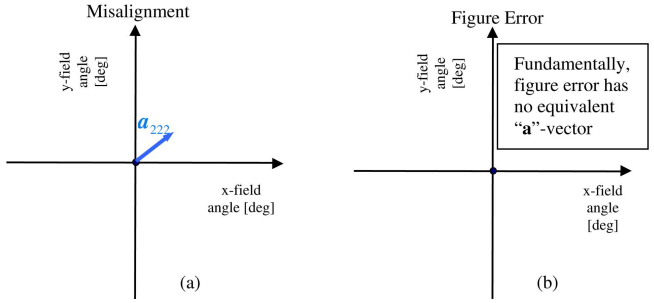

Fig. 7. The vector $\boldsymbol{a}_{222}$ that locates the center of biplanar symmetry of the binodal astigmatic field for a Ritchey-Chrétien telescope with secondary misalignment and primary mirror astigmatic figure error. (a) Contribution from secondary mirror misalignments under the condition that field-constant coma has been removed, and (b) the contribution from astigmatic figure error on the primary mirror, as derived in Section 2 and 3, has no $\boldsymbol{a}_{222}$ component.

#128812 - $15.00 USD Received 21 May 2010; revised 3 Jul 2010; accepted 13 Jul 2010; published 30 Jul 2010

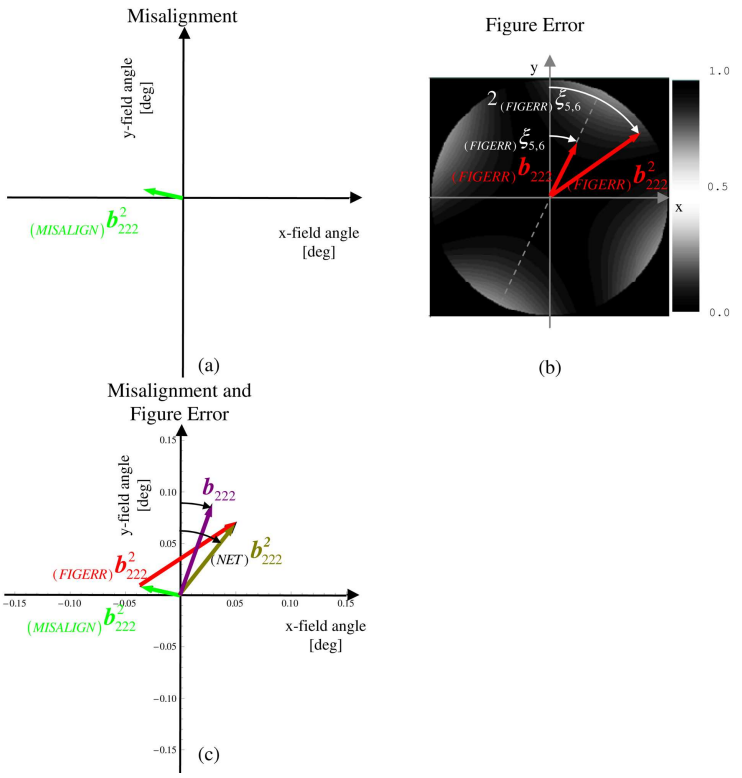

Fig. 8. The vector $\boldsymbol{b}_{222}$ that points then as $\pm i\boldsymbol{b}_{222}$ from the endpoint of $\boldsymbol{a}_{222}$ to the nodal points for binodal astigmatism, shown here for a Ritchey-Chrétien telescope with secondary misalignment and primary mirror astigmatic figure error, consisting of (a) ${}_{(ALI)}\boldsymbol{b}^2_{222}$, denoting the contribution caused by secondary mirror misalignments, (b) ${}_{(FIG)}\boldsymbol{b}^2_{222}$ determined by interferogram data, combined with the knowledge of the total astigmatism in the nominal optical system, resulting in (c) the overall vector $\boldsymbol{b}^2_{222}$ and $\boldsymbol{b}_{222}$ the final astigmatic node locating vector, when combined with $\boldsymbol{a}_{222}$.

Figure 9 presents the most important graphical realization for the results of this paper. In Fig. 9(a) the nominal astigmatic aberration field is shown, having the two astigmatic nodes coincide at the field center, and in Fig. 9(b) the general nodal symmetry for the case of misalignments only, for the condition where axial (field constant) coma has been removed is shown. The general feature to be recognized here is that one of the astigmatic nodes is located at the field center, which has been shown to be a direct consequence of removing misalignment induced field-constant coma [8]. In comparison, Fig. 9(c) demonstrates the effects of astigmatic figure error on the 3rd order astigmatic aberration field, which demonstrates that the nodes are constrained to remain symmetric with respect to the field center (here the telescope is otherwise perfectly aligned). Figure 9(d) combines the two sources of degradation, secondary misalignments and primary mirror astigmatic figure error. It can be observed that the binodal field dependence displays symmetry about the field point denoted by the vector $\boldsymbol{a}_{222}$.

Another property of the aberration field vectors $\boldsymbol{a}_{222}$ and $\pm i\boldsymbol{b}_{222}$ becomes apparent when comparing Fig. 9(b) with Fig. 9(d). While in the absence of misalignment induced field-constant coma and astigmatic figure errors the direction of the node splitting always occurs

#128812 - $15.00 USD Received 21 May 2010; revised 3 Jul 2010; accepted 13 Jul 2010; published 30 Jul 2010

along the orientation of the vector $\boldsymbol{a}_{222}$ (Fig. 9(b)), this constraint is removed in the presence of astigmatic figure errors (Fig. 9(d)). With these new insights into these fundamental nodal properties of astigmatism, it becomes apparent that measuring non-zero astigmatism at the field center can only be caused by an astigmatic figure error, since in the case of pure misalignments one astigmatic node will remain at the field center causing misalignment induced astigmatism to be effectively zero. Consequently, measuring astigmatism at the field center (where the field center is determined independently based on the measurement or control of boresight error) would completely quantify an astigmatic figure error, even in the presence of secondary mirror misalignments. Knowing the behavior of astigmatism, as described mathematically in Eq. (9)-(16) is valuable because the astigmatic nodal positions are readily found from as few as three measurements of the wavefront at different points in the field of view in some metric that can be reduced to Zernike coefficient terms. Given the nodal positions, with the special configurations highlighted in Figs. 9(b), 9(c), it can be determined if secondary mirror misalignment, astigmatic figure, or a combination of both is present simultaneously. If neither astigmatic node is effectively on-axis and if the nodes are not symmetrically placed about the axis then both types of errors are present and can be extracted independently. The magnitude of astigmatism versus field, corresponding to Figs. 9(a)-9(d), is visualized in Figs. 10(a)-10(d).

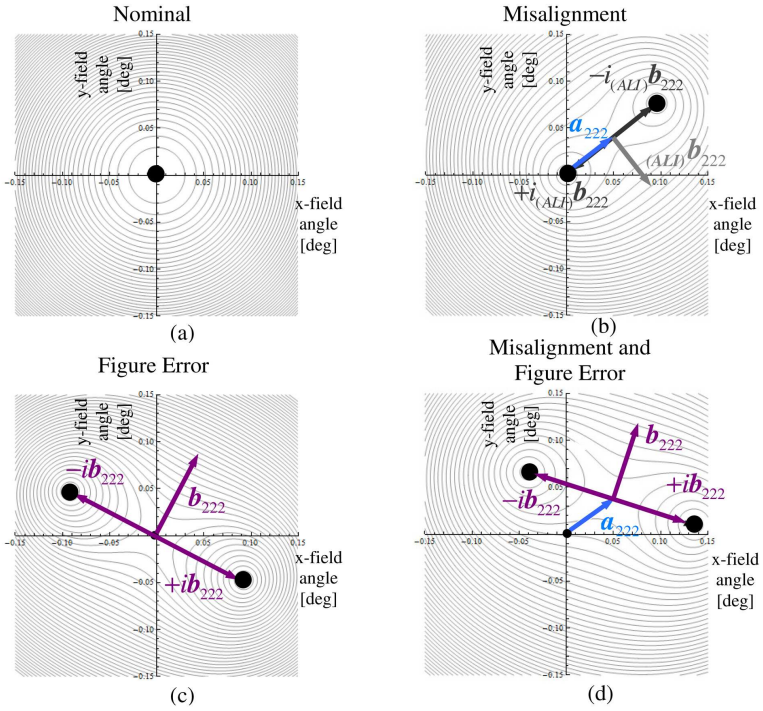

Fig. 9. The characteristic node geometry for (a) the nominal astigmatic aberration field, exhibiting purely quadratic astigmatism, (b) misalignment induced binodal astigmatism, (c) astigmatic figure error induced binodal astigmatism, and (d) both contributions, (b) and (c) combined.

#128812 - $15.00 USD Received 21 May 2010; revised 3 Jul 2010; accepted 13 Jul 2010; published 30 Jul 2010

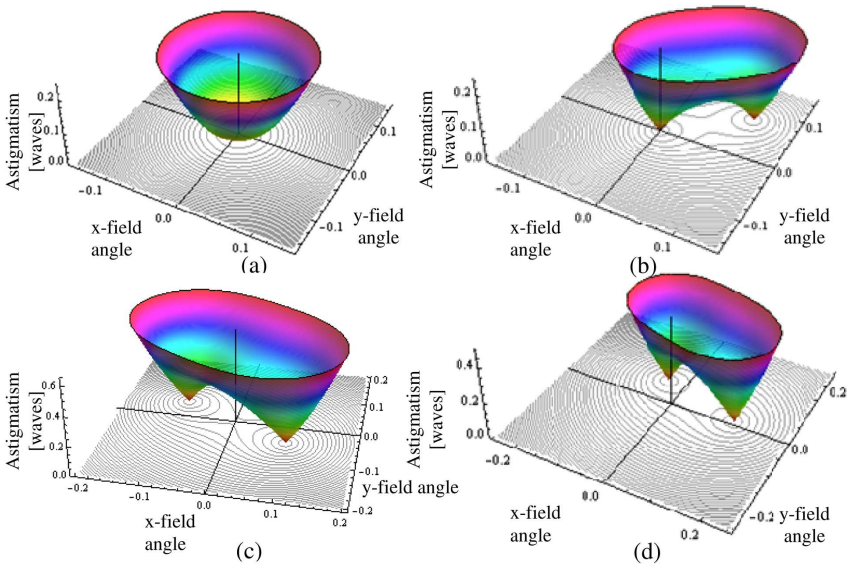

Fig. 10. Magnitude of astigmatism of (a) the nominal Ritchey-Chrétien telescope, (b) binodal astigmatism in the presence of misalignments after alignment to remove constant coma, (c) an aligned telescope with only astigmatic figure error, (d) combined misalignments (b) and astigmatic figure error (c).

5. Validation of the nodal properties of a Ritchey-Chrétien telescope with misalignments and astigmatic figure error

To validate the predicted nodal behavior of astigmatism as shown in Fig. 9 and Fig. 10, Full-Field-Displays (FFDs) for the astigmatic line images for an aligned telescope, alignment errors alone, figure errors alone, and the simultaneous combination of errors are shown in Fig. 11(a)-11(d), respectively. Comparing the node locations predicted by nodal aberration theory and real-raytrace data in all cases has demonstrated excellent agreement. Here Fig. 9(a) and Fig. 11(a) compare the aligned state of the telescope. Additionally, Fig. 9(b) (generated with Eq. (11)-(16)) and Fig. 11(b) (Coddington raytrace in commercial optical design software) show the astigmatic node locations in the presence of misalignments only. Similarly, Fig. 9(c) (generated with Eq. (17)) corresponds to the case shown in Fig. 11(c) (Coddington raytrace in optical design software), visualizing the case where only astigmatic figure errors are present, and the node locations in the presence of combined misalignments and astigmatic figure error are shown in 9d (generated with Eq. (10)-(16)) and verified with the FFD in Fig. 11(d).

Even though not obvious from visually comparing Fig. 11(c) and Fig. 11(d), a quantitative comparison of the FRINGE Zernike coefficients at the field center (i.e. x-field = y-field = 0) reveals identical values for Z_5 and Z_6, confirming the predicted behavior with nodal theory. It is important to recognize that while FFDs were developed to illustrate the nodal aberration field behavior, is it simply a display method. The data that is being displayed is based on real ray tracing, with no "knowledge" of nodal aberration theory. As a result this is an excellent validation of the theoretical developments presented here.

#128812 - $15.00 USD Received 21 May 2010; revised 3 Jul 2010; accepted 13 Jul 2010; published 30 Jul 2010

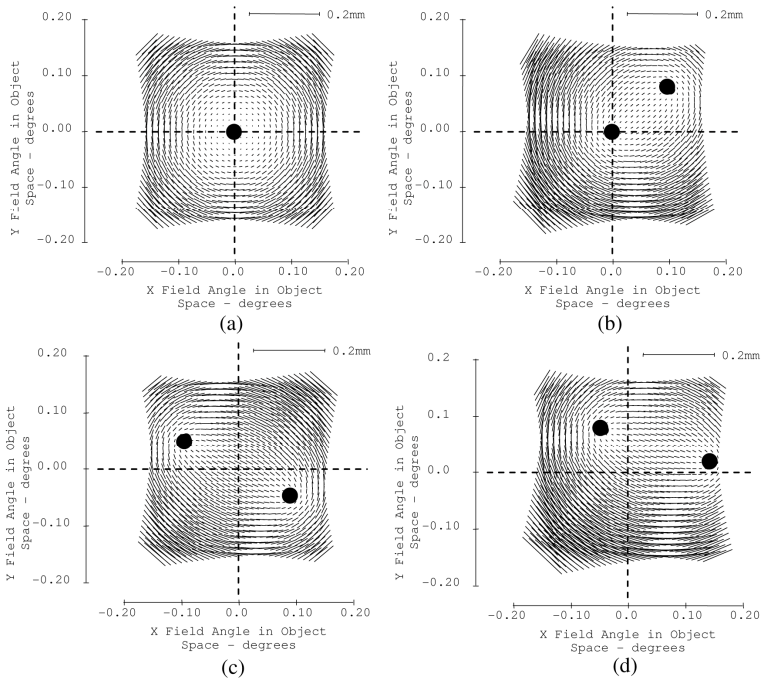

Fig. 11. A Real-Ray based verification of the prediction of astigmatic nodal positions by a generalized Coddington close skew ray trace, illustrating the (a) nominal astigmatic aberration field, exhibiting purely quadratic astigmatism with two coincident astigmatic nodes at the field center, (b) node positions for secondary mirror misalignments only, in a configuration that is corrected for zero field-constant coma, (c) node positions corresponding to the astigmatic figure error illustrated in Figs. 8(b), and 8(d) net display including the secondary misalignments and astigmatic figure error.

6. Conclusion

We have presented an important extension to nodal aberration theory; the integration of astigmatic primary mirror figure errors to the existing theory that was previously developed only for rotationally symmetric surfaces that have been misaligned. This extension has led directly to a method for separating misalignment induced astigmatism from astigmatic figure errors in Ritchey-Chrétien telescopes. The key insight to accomplish this distinction is to recognize that after aligning the telescope for zero field-constant (axial) coma, one astigmatic node remains effectively at the field center when there is no astigmatic figure error, as detailed in [8]. Consequently, measuring astigmatism at the center of the field directly reveals the existence of an astigmatic figure component on the primary mirror. Here, to highlight the important concepts it is assumed that the telescope boresight error is established independent of the nodal properties. The property that the midpoint between the astigmatic nodes, located by $\boldsymbol{a}_{222}$, has no component due to figure error can be utilized to separate astigmatic figure from misalignment induced astigmatism. This separation has emerged as a key aspect of the optimal operation of active mirror components that are rapidly becoming standard equipment on large astronomical telescopes.

With this extension to nodal aberration theory, it is possible to minimize or even eliminate the use of the dynamic range of the active optics system on aberrations that are better controlled by alignment. While the theory has been demonstrated for the important case of a Ritchey-Chrétien telescope (with the aperture stop at the primary mirror), these developments are being extended to any optical system, where the location of the surface with figure errors does not have to be at a stop surface. The analytical predictions for the astigmatic node

#128812 - $15.00 USD Received 21 May 2010; revised 3 Jul 2010; accepted 13 Jul 2010; published 30 Jul 2010

locations in the presence of misalignments and astigmatic figure errors at the stop surface have been compared to results obtained from optical design software, and excellent agreement has been found, as illustrated in Fig. 11. The theory provided can directly be leveraged in the development of alignment strategies for optical systems.

Acknowledgements

We would like to thank Optical Research Associates for providing an educational license for CODE V®, which enabled this work. This research was funded by the Florida I-4 Corridor and the NYSTAR Foundation.

#128812 - $15.00 USD Received 21 May 2010; revised 3 Jul 2010; accepted 13 Jul 2010; published 30 Jul 2010